CRREL REPORT 94-13

Analyzing the Stability of Floating Ice Floes

Barry Coutermarsh and Randy McGilvary

December 1994

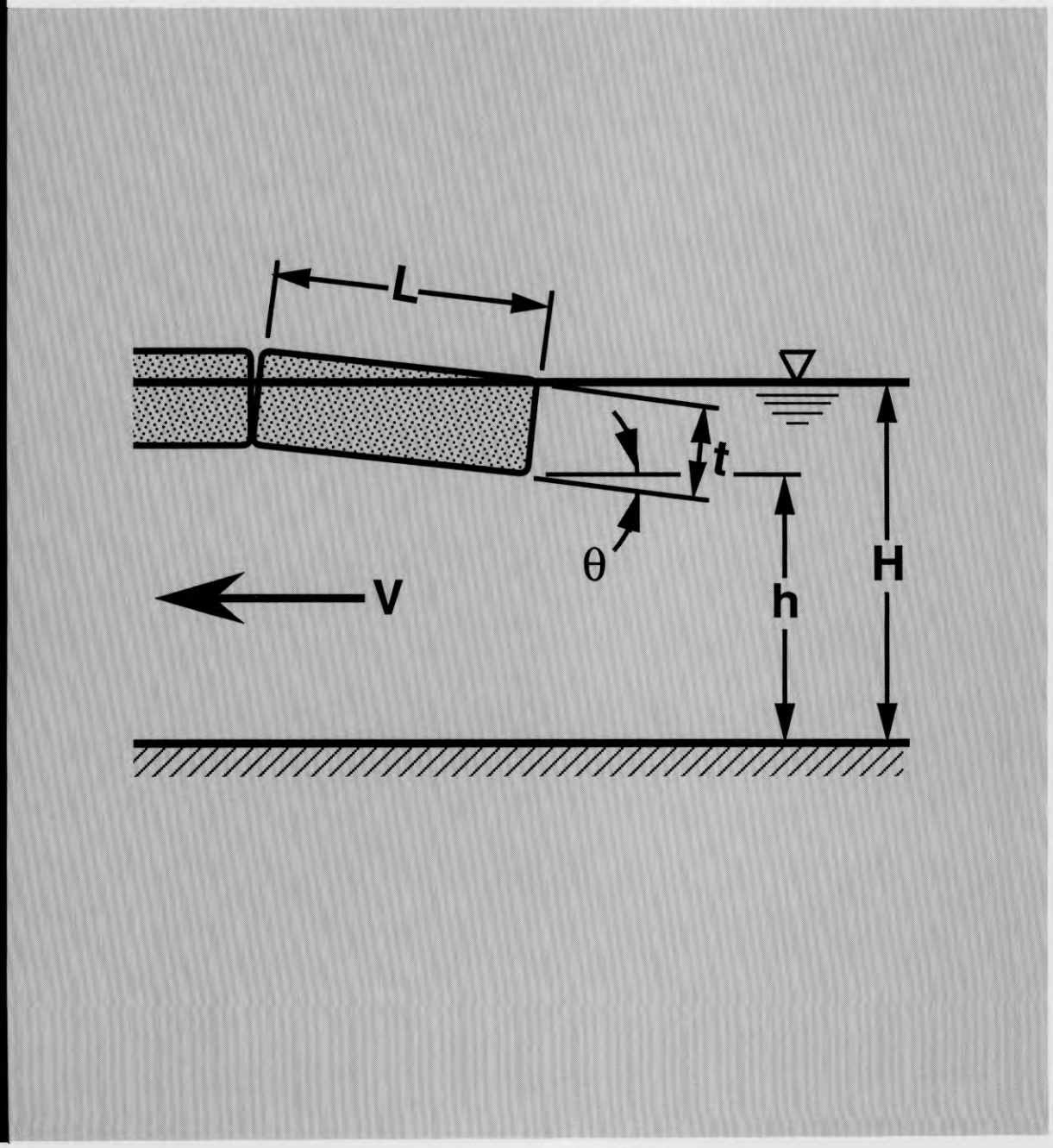

Abstract

This report describes an experimental study to measure the pressure caused by fluid acceleration beneath a floating parallelepiped block. Dynamic fluid pressure was measured at discrete points beneath the block for several flow velocities, flow depths, block angles of attack and block-thickness-to-depth ratios. The measured pressures were used to calculate block underturning moments, and a hydrostatic analysis was used to calculate a block righting moment. From this, a densimetric Froude underturning criterion is presented. The measured hydrodynamic pressure distribution on the bottom of a single model ice floe is used to estimate the dynamic stability at three thickness-to-depth ratios. The energy-based analysis details the conditions required for instability, metastability and stability. At three thickness-to-depth ratios, block rotational inertia has the effect of reducing the Froude stability number by 5 to 10% over a completely static stability criterion.

Cover: Underturning block (L = block length; V = fluid velocity; θ = rotation angle; t = block thickness; H = flow depth).

For conversion of SI metric units to U.S./British customary units of measurement consult ASTM Standard E380-89a, *Standard Practice for Use of the International System of Units,* published by the American Society for Testing and Materials, 1916 Race St., Philadelphia, Pa. 19103.

CRREL Report 94-13

US Army Corps of Engineers
Cold Regions Research & Engineering Laboratory

Analyzing the Stability of Floating Ice Floes

Barry Coutermarsh and Randy McGilvary

December 1994

PREFACE

This report was prepared by Barry Coutermarsh, Research Civil Engineer, Applied Research Branch, and Randy McGilvary, Research Hydraulic Engineer, Ice Engineering Research Branch, Experimental Engineering Division, U.S. Army Cold Regions Research and Engineering Laboratory.

The authors thank Dr. E. Marvin at CRREL for facilitating the funding for this work. Technical review of this report was provided by Dr. J.-C. Tatinclaux and S.F. Daly, both of CRREL.

CONTENTS

ILLUSTRATIONS

Figure

TABLES

NOMENCLATURE

A	block plane area
C	dynamic fluid pressure coefficient
$C(\theta^*)$	dynamic fluid pressure coefficient at the angle of maximum hydrostatic righting moment
COP_X	center of pressure in the X-direction (across block width)
COP_Y	center of pressure in the Y-direction (along block length)
F	force
F_r	densimetric Froude number
F_r^*	critical densimetric Froude number for block stability
g	acceleration due to gravity
H	flow depth upstream from the block
I	moment of inertia
L	block length
M	moment acting on the block
M_f	underturning moment created by fluid flow
$M_f(\theta)$	underturning moment created by fluid flow at an angle of attack
$M_f(\theta^*)$	underturning moment created by fluid flow at angle of maximum righting moment
M_r	hydrostatic righting moment
$M_r(\theta)$	hydrostatic righting moment at an angle of attack
$M_r(\theta^*)$	hydrostatic righting moment at angle of maximum righting moment
M_u	underturning moment in the Y-direction
M_X	underturning moment about X-axis
M_Y	underturning moment about Y-axis
M_{max}	maximum hydrostatic righting moment
$P(X,Y)$	differential pressure from hydrostatic at a point (X,Y)
$\overline{P}$	mean differential pressure from hydrostatic
S_t	Strouhal number
t'	block freeboard
t	block thickness
V	fluid velocity upstream from the block
V^*	approach velocity of instability
X	spatial coordinate, distance across block width
Y	spatial coordinate, distance along block length
Z	spatial coordinate, distance perpendicular to X–Y plane
α	nondimensional moment coefficient in Y-direction
$\alpha(\theta^*)$	nondimensional moment coefficient in Y-direction at maximum righting moment angle
ρ	fluid density
ρ'	block density
ρ_i	ice density
ρ_w	water density
θ	block angle of attack (rotation) from horizontal
θ^*	block angle of attack at the angle of maximum righting moment
θ_0	initial block angle
$\dot{\theta}$	block angle velocity
$\ddot{\theta}$	block angular acceleration

Analyzing the Stability of Floating Ice Floes

BARRY COUTERMARSH AND RANDY MCGILVARY

INTRODUCTION

Ice floes that come to rest against an obstruction, such as an ice boom or an intact ice sheet, either will remain there or underturn. Floes that do not underturn become part of an ice cover that progresses upstream, while floes that underturn may become lodged beneath the downstream cover and contribute to the growth of an ice jam. It is for these reasons that block underturning has been studied to help us understand the conditions that affect ice floe stability. Figure 1 is a schematic diagram of the physical situation that defines important variables.

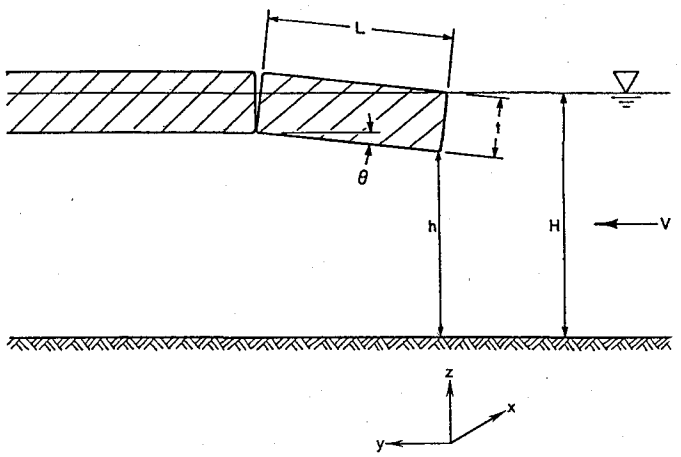

Figure 1. Underturning block problem.

Of the studies that examined block stability criteria, most have assumed simple empirical descriptions for the forces and moments caused by fluid acceleration around the floating block. In this study, we measured the actual pressures acting on the bottom surface of a floating block, considering the effects of flow velocity, flow depth and block angle of attack on the pressure distribution. These measured pressures were both positive (stabilizing) and negative (destabilizing), depending primarily upon the angle of attack. The resulting integrated force magnitude and center of pressure locations were used to calculate the total resultant underturning moment acting on the block. To simplify the experiment, we used a rigidly supported block to eliminate the higher order dynamics associated with block rotation, such as the fluid added mass, block rotational inertia and the changing relative velocity between the fluid and the block.

We compare the block's buoyancy-induced righting moment as a function of attack angle with the underturning moment to determine the conditions when the underturning moment would exceed the righting moment and the block would underturn. From this, we propose a simple stability criterion that relates the block densimetric Froude number to a dimensionless moment coefficient at the angle of maximum righting moment.

We then use the measured hydrodynamic pressures to estimate the dynamic stability at three thickness-to-depth ratios. This energy-based analysis details the conditions required for instability, metastability and stability. We show that, at all three thickness-to-depth ratios, block rotational inertia reduces the stability Froude number by 5 to 10% over a completely static stability criterion.

BACKGROUND

Literature cited

Past investigators have assumed a uniformly distributed underturning pressure across the block and conducted static analyses on data that included block angular acceleration and angular velocity. Perhaps the most popular stability criterion was that of Pariset and Hausser (1961), who assumed that ice floes would become unstable when the upstream edge lost its freeboard. This incipient instability condition became known as the "no-spill criterion."

Uzuner and Kennedy (1972) developed an underturning criterion where block rotation was the primary mechanism. Their analysis included an empirical moment coefficient that depended upon t/L

and ρ'/ρ_w and was determined by disregarding the effect of t/H (where t is the block thickness, L the block length, H the upstream flow depth, ρ' the block density and ρ_w the fluid density). They also defined a "no-spill" condition as the point at which the upstream top corner of the block was lowered to the stagnation height of the water surface, and they declared this to be the point of instability.

Ashton (1974) employed the "no-spill" criterion, finding a vital dependence upon block thickness and block thickness-to-depth ratio. But he believed that thickness-to-length ratio was of little importance, as was depth alone, although he noted a slight increase in instability with increasing thickness-to-length ratios. He also provided a simplified moment analysis, taking into account the block weight, global fluid acceleration to maintain continuity and the displaced volume of fluid. In his analysis the hydrostatic righting moment was proportional to the sine of the angle of block rotation, with the moment assumed to act at $L/2$ and with an implicitly assumed lift coefficient of 1.

Coutermarsh (1986) studied ice floes striking against the 45° sloped face of a military floating bridge to see if they would jam or underturn. That situation was very similar to the one we're concerned with here, except that the block rotated about its upper downstream corner, a factor that made a minimal difference in the analysis. That study, however, pointed out that the underturning phenomenon was poorly described for the deep water region and that no one previous study had described instability over both the deep and shallow water regions.

Daly and Axelson (1990) performed detailed calculations to determine the hydrostatic righting moment related to the displaced volume of the block as it rotates. They found this righting moment to be highest at an angle that depended on block density, thickness and length. They reasoned that the block became unstable when the underturning moment caused by the fluid flow was greater than the maximum righting moment; they discounted the previous notion of the "no-spill" condition. Their analysis also determined a moment coefficient that included two empirically determined parameters found through analysis of existing laboratory data.

Analytical discussion

We approach our block instability study by following past convention and assume that the block rotates about its lower downstream corner because of a pressure reduction at the bottom surface of the block. This pressure reduction creates moments about the X-axis (parallel to the stream flow) and about the Y-axis (transverse to the stream flow) that would be calculated as

$$M_X = \int_A P(X,Y) Y \, dA \tag{1}$$

$$M_Y = \int_A P(X,Y) X \, dA \tag{2}$$

where $P(X,Y)$ is the pressure differential from hydrostatic and A is the block plane area.

With the total force at the bottom surface as

$$F = \int_A P(X,Y) \, dA \tag{3}$$

the average pressure is

$$\overline{P} = F/A. \tag{4}$$

We define a dynamic fluid pressure coefficient (Euler number or lift coefficient) as

$$C = \frac{\overline{P}}{\frac{1}{2}\rho_w V^2} \tag{5}$$

with ρ_w being water density and V flow velocity upstream of the block. The centers of pressure in the $X(COP_X)$ and $Y(COP_Y)$ directions are

$$COP_X = \frac{M_y}{F} \tag{6}$$

$$COP_Y = \frac{M_x}{F}. \tag{7}$$

In our study we were only concerned with the Y-direction moments and forces, as they are the ones that will contribute to underturning. If symmetry is present about the Y-axis, the X moments will balance, i.e., the block will not tend to rotate around the Y-axis. We, therefore, define a nondimensional moment coefficient α in the Y-direction as

$$\alpha = C\left(\frac{COP}{L}\right) \tag{8}$$

or alternatively

$$\alpha = \frac{M_x}{\frac{1}{2}\rho_w V^2 AL} \tag{9}$$

where L = floe length
C = lift coefficient
COP/L = center of pressure normalized against the block length.

The subscript Y has been dropped from the COP here (eq 8). These parameters are related to the aver-

age pressure acting on the block underside $\overline{P}$ by eq 5 and

$$\left(\frac{COP}{L}\right)=\frac{M_u}{PAL} \tag{10}$$

where M_u is the underturning moment in the Y-direction.

In addition to the forces working to underturn the block, there is a hydrostatic righting moment that depends on fluid density, block density, length, thickness and angle of rotation. Daly and Axelson (1990) showed that the righting moment for a parallelepiped block is represented by

$$\frac{M_u}{\frac{1}{2}\rho_w\, gtA}=t'\sin(\theta)\,(\rho'-1)+\rho'(\sec(\theta)-1)$$

$$\left[t'\tan(\theta)+(t'-L\tan(\theta))\sin(\theta)+L\sec(\theta)\right]$$

$$+\frac{L}{t}\tan^2(\theta)\left(t'+\frac{2L}{3}\csc(\theta)-\frac{L}{3}\sin(\theta)\right) \tag{11a}$$

for $0 \le \theta \le \theta_1$ and

$$\frac{M_r}{\frac{1}{2}\rho_w\, gtA}=(L\cos(\theta)+t\sin(\theta))(1-\rho')$$

$$-\frac{t}{L}(1-\rho'\sec(\theta))^2\left(t'+\frac{1}{3}(t\cos(\theta)\right.$$

$$\left.-t')\left(\csc^2(\theta)+1\right)\right) \tag{11b}$$

for $\theta_1 \le \theta \le \theta_2$ and

$$M_r=\frac{1}{2}(\rho_w-\rho_i)\, gtA$$

$$(L\cos(\theta)+t\sin(\theta)) \tag{11c}$$

for $\theta_2 \le \theta \le \pi/2$

where

$$\rho'=\frac{\rho_i}{\rho_w} \tag{12a}$$

$$t'=\frac{\rho_i}{\rho_w}t \tag{12b}$$

$$\theta_1=\sin^{-1}\left\{\frac{\left[\left(\frac{L}{t}\right)^2-(\rho')^2+1\right]^{\frac{1}{2}}-\rho'\frac{L}{t}}{\left(\frac{L}{t}\right)^2+1}\right\} \tag{12c}$$

$$\theta_2=\cos^{-1}[\rho'] \tag{12d}$$

and t = block thickness
ρ_i = ice density
g = acceleration of gravity
θ_1 = angle at which the leading edge loses its freeboard
θ_2 = angle at which the trailing edge loses its freeboard.

Daly and Axelson calculated this moment for both floating and submerged blocks, but the form of the equations they presented made it difficult to determine the magnitude and reaction point of the righting force. To determine these components, we calculated the hydrostatic righting moment through the use of hydrostatic pressure prisms (Streeter and Wylie 1979). These lead to the nondimensional hydrostatic moment given as a function of length to thickness, as shown in Figure 2. Note that for lengths in excess of about five thicknesses, the maximum hydrostatic righting moment may be approximated by

$$M_{max} \approx (1-\rho_i/\rho_w)\,\rho_w\, gtA\,(L/2)\,. \tag{13}$$

In addition, the angle of maximum hydrostatic righting moment θ^* is shown in Figure 2, and for lengths greater than about 2.5 thicknesses may be approximated as

$$\theta^* \approx \tan^{-1}[t/L]\,. \tag{14}$$

We have also plotted the previously used "no-spill" angle criterion in Figure 2 for comparison. It is important to note that the no-spill angle is significantly smaller than the angle at which the maximum righting moment occurs. For our particular block, the hydrostatic righting moment is shown in Figure 3 for t = 0.076 m and L = 0.62 m. Our block-length-to-thickness ratio is 8 and the approximations to the maximum righting moment and angle of maximum righting moment are in very good agreement with the actual values.

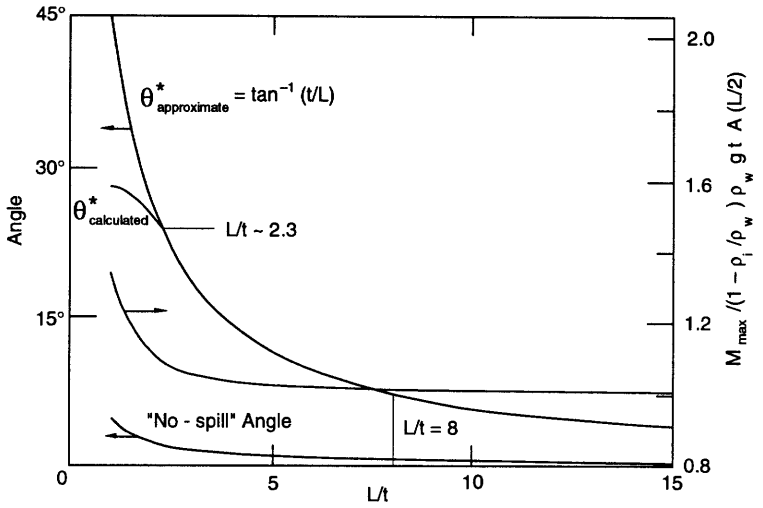

Figure 2. Hydrostatic righting moment. Both the calculated and approximate angle at which the maximum hydrostatic righting moment occurs are plotted vs. the block-length-to-thickness ratio. Our block L/t = 8. Also shown is the previously used "no-spill" angle condition for block instability.

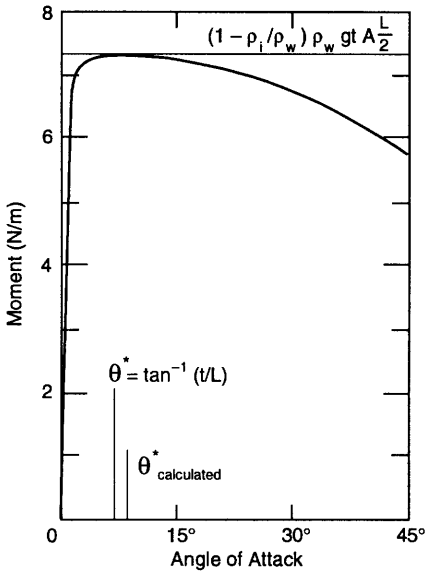

Figure 3. Calculated block hydrostatic righting moment for our particular block vs. angle of attack. Both the calculated and approximate angles of maximum righting moment are also shown. The horizontal line is the approximated maximum righting moment for our block.

EXPERIMENTAL METHODS

Objective

Our objective was to measure the pressures acting on the block. As Daly and Axelson (1990) pointed out, most of the previous work has implicitly assumed that the flow beneath a block is one-dimensional, resulting in a uniform dynamic pressure. (Larsen [1975] assumed a two-dimensional, inviscid, irrotational flow to calculate a one-dimensional pressure variation on the block underside.) We felt that three-dimensional flow, producing the two-dimensional pressure distribution on the block, better represented actual conditions. Furthermore, we assumed that the flow pattern would be primarily influenced by flow depth, block thickness and block angle of attack. We also believed that it was necessary to characterize the fluid dynamic pressure by calculating both the average pressure magnitude and center of pressure on the block bottom surface for several attack angles, from horizontal through the angle of maximum hydrostatic righting moment.

Setup

The experiments were conducted in CRREL's warm flume, having a cross section of 0.91 by 0.91 m, a total length of 7.32 m and a variable pumping capacity up to 0.3 m^3/s. A hollow Plexiglas block "ice floe," 61.6 cm square by 7.62 cm thick, was constructed with 91 pressure taps in its bottom surface. The taps were sized to accept 6.35-mm o.d. polyethylene manometer tubing and were variably spaced as shown in Figure 4. A Plexiglas cover extended over the top front half to keep water from hitting the tubes as the block front submerged during rotation. The block was fastened to the flume by hinged supports at its rear and an adjustable threaded rod at its front top (Fig. 5).

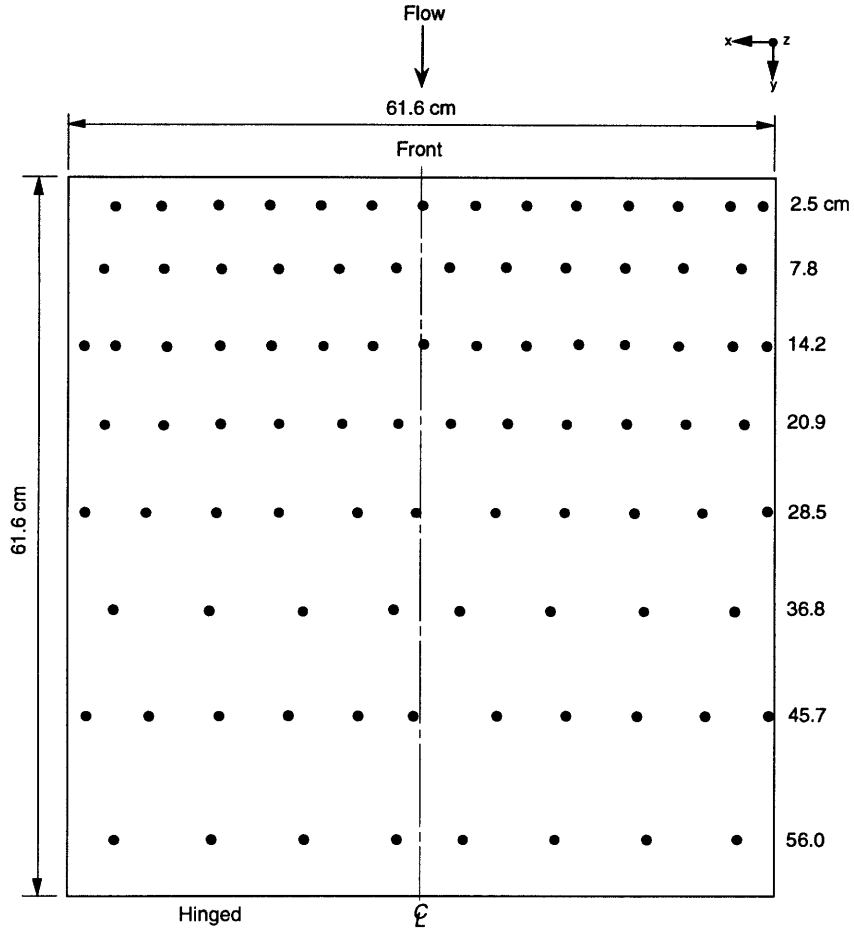

Figure 4. Tap locations. They were variably spaced in both the X and Y directions.

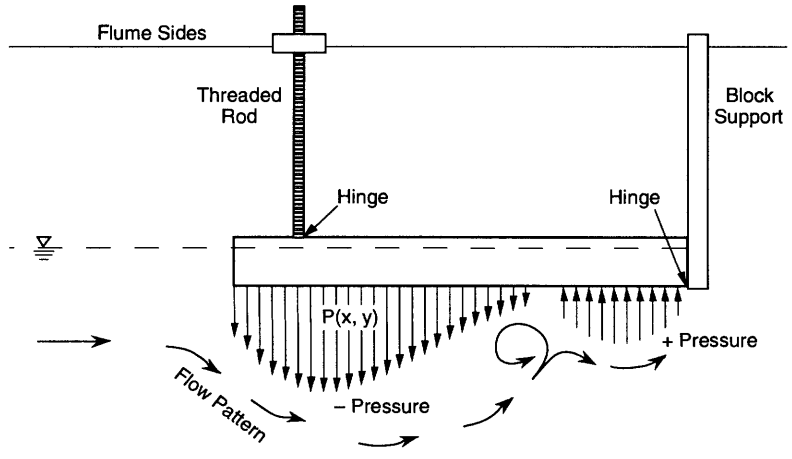

Figure 5. Block attached to the flume at the front by a threaded rod and at the rear by hinged supports. These held the block rigid during a test but still allowed the attack angle to be changed.

This allowed both vertical and rotational (angle of attack) adjustments.

Pressure was measured by routing 24 water-filled manometer tubes via a fluid switch multiplexer to a liquid-to-gas pressure transducer that had a ±6.35-cm range. In this manner it was possible to measure the pressure of 24 separate manometer taps with one transducer. A stilling tube gave us a stable measure of the piezometric head in the flume, which was measured at the beginning and end of each group of readings. In this way the dynamic fluid pressure difference from static was determined

Table 1. Test matrix showing thickness-to-depth ratios (*t/H*), velocities (*V*) and angles of attack used.

t/H	*Velocity* V *(m/s)*				*Angle of attack (degrees)*						
0.10	0.45				0.0	3.3	6.6	10.0	13.4	16.8	20.4
0.13	0.14*	0.23	0.39	0.50	0.0*	3.3	6.6	10.0	13.4	16.8	20.4
0.20	0.39**	0.50	0.60		0.00**	1.1	3.3	6.6	10.0	13.4	16.8

* One test at $t/H = 0.13$, $V = 0.14$, and 0° angle of attack
** Four tests at $t/H = 0.20$, $V = 0.39$, and 0° angle of attack

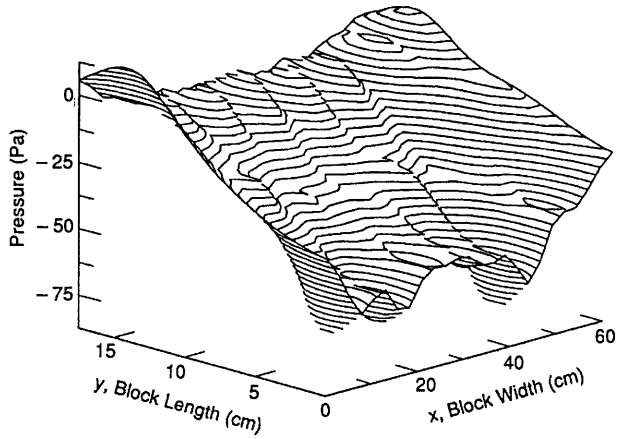

Figure 6. Surface plot showing a typical pressure distribution across the full width of our block during a symmetry check. Only the first three rows of taps were used; V = *0.35 m/s,* t/H = *0.05 and* θ = *0°.*

for each tap. The readings and their standard deviations were plotted in real-time and stored on a personal computer.

Test procedure

We began a typical test by setting the water to the desired depth and horizontally submerging the block to the required displacement. The flume velocity was adjusted to the desired value and two scans of 25 pressures (two for static height and 23 taps) were made. The model floe was rotated to the next desired angle and two more scans made. This procedure was repeated until all desired block angles were examined for any given depth and velocity.

We did the experiments in two phases. The first was to verify the symmetry of the pressures across the full width of the block. The second was to measure pressures on one half of the block, assuming symmetry of the pressure distribution for the other half.

RESULTS

Phase one

A typical pressure distribution obtained during phase one of our experimental program is shown in Figure 6. The water flow was in the positive Y-direction. The readings were obtained at a zero angle of attack and a velocity of 0.35 m/s. In these experiments, a negative pressure tended to rotate the block downward, i.e., toward the negative Z-direction; a positive pressure pushed against the block in the positive Z-direction. Examination of the figure points out the pressure distribution's high degree of symmetry about the block centerline at $X = 30.5$ cm. Having proven symmetry, we instrumented one half of the block along its entire length, and entered the second phase of the experimental program.

Phase two

The experiments were run at three values of t/H—0.10, 0.13 and 0.20—and were obtained from our fixed block thickness of 7.62 cm and three different flow depths. Velocities used were 0.14, 0.23, 0.39, 0.45, 0.50 and 0.60 m/s (Table 1). Block attack angles ranged from 0° to approximately 20°. Two replicates were performed at each condition, except as noted in Table 1, and the data presented below are the average of these two replicates.

Figure 7 illustrates a typical surface pressure plot obtained during phase two. Generally, at zero angle of attack, the pressures were lower at the front of the block, becoming less negative, if not positive, towards the rear of the block. The rear central portion of the block was frequently near zero pressure, with perhaps some areas of negative pressure at the cor-

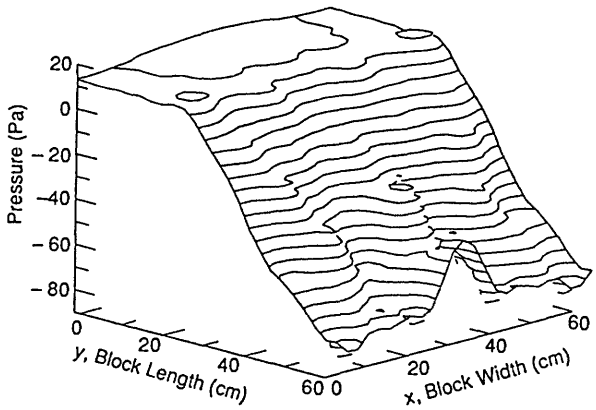

Figure 7. Typical pressure distribution surface plot. This is created by reading selected taps along one side of the block and generating a mirror image of the pressures on the opposite side. In this example V = *0.39 m/s,* t/H = *0.13 and* θ = *0°.*

ners. The pressure at the front central portion of the block was frequently less negative than at the front sides or the block's midsection. As the angle of attack increased, the magnitude and area of negative pressure would increase and move towards the rear of the block until eventually the entire pressure distribution was negative. Figure 8 shows typical pressure distributions from our tests: those from test 1 ($t/H = 0.10$) tended to be more uniform between the front and rear sections of the block than those from tests 2 and 3 (t/H = 0.13 and 0.20 respectively). In test 3 the pressure difference between the front and rear sections of the block is greater and the overall pressure is lower. There are also numerous areas of extremely low pressure, probably associated with vortex formation and flow separation.

To characterize the pressure distributions, we calculated the surface area over which the pressure acts and the average for regions of positive and negative pressure (Fig. 9). It is interesting that tests 1 and 3 have roughly the same area of negative pressure, with a much greater magnitude for test 3.

Figure 10 shows the positive and negative center of pressure (*COP*) locations (measured from the rotation axis) and the resultant moment for each test. Here, it can be seen that, although test 2 did not have quite the area of negative pressure that test 1 did, its negative *COP* is farther from the axis of rotation, while its positive *COP* is about the same as test 1's. This results in the two moments being very similar in the initial stages of rotation, with test 2's being greater at the higher attack angles where the effect of depth is probably being felt. Test 3 has a much higher moment than the others, but its negative *COP* is almost identical to test 1's. It should be noted

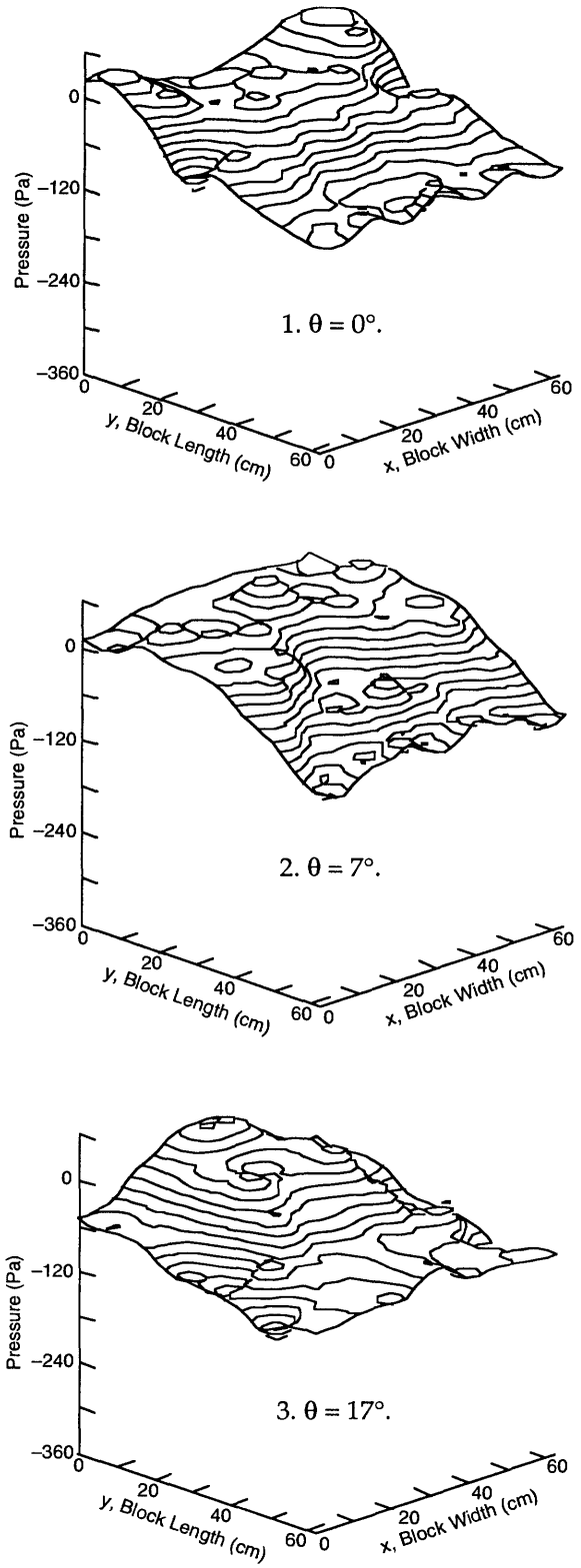

a. Test 1: t/H = *0.10,* V = *0.45 m/s.*

Figure 8. Representative pressure distributions from three tests. The block's trailing edge is at Y = *0.*

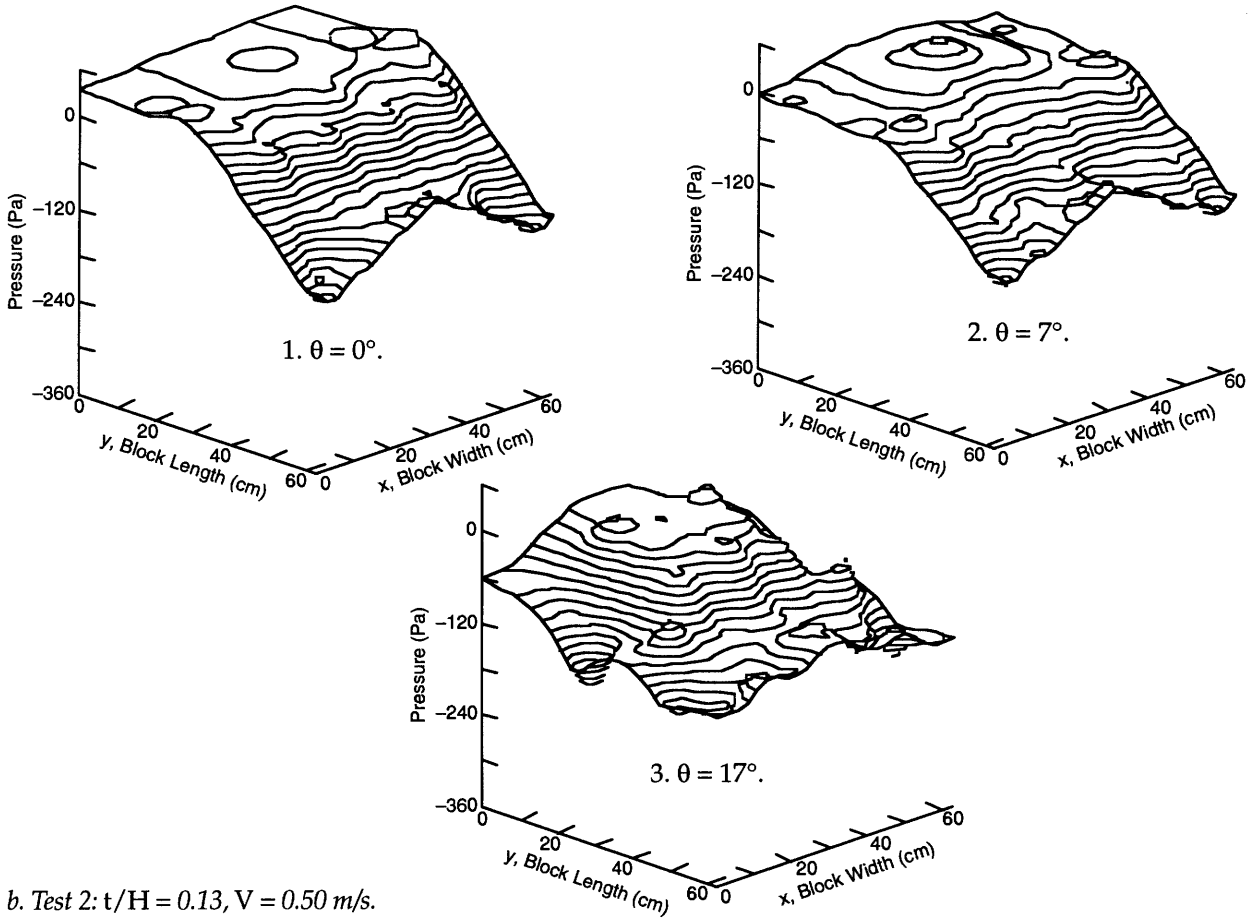

b. Test 2: t/H = *0.13,* V = *0.50 m/s.*

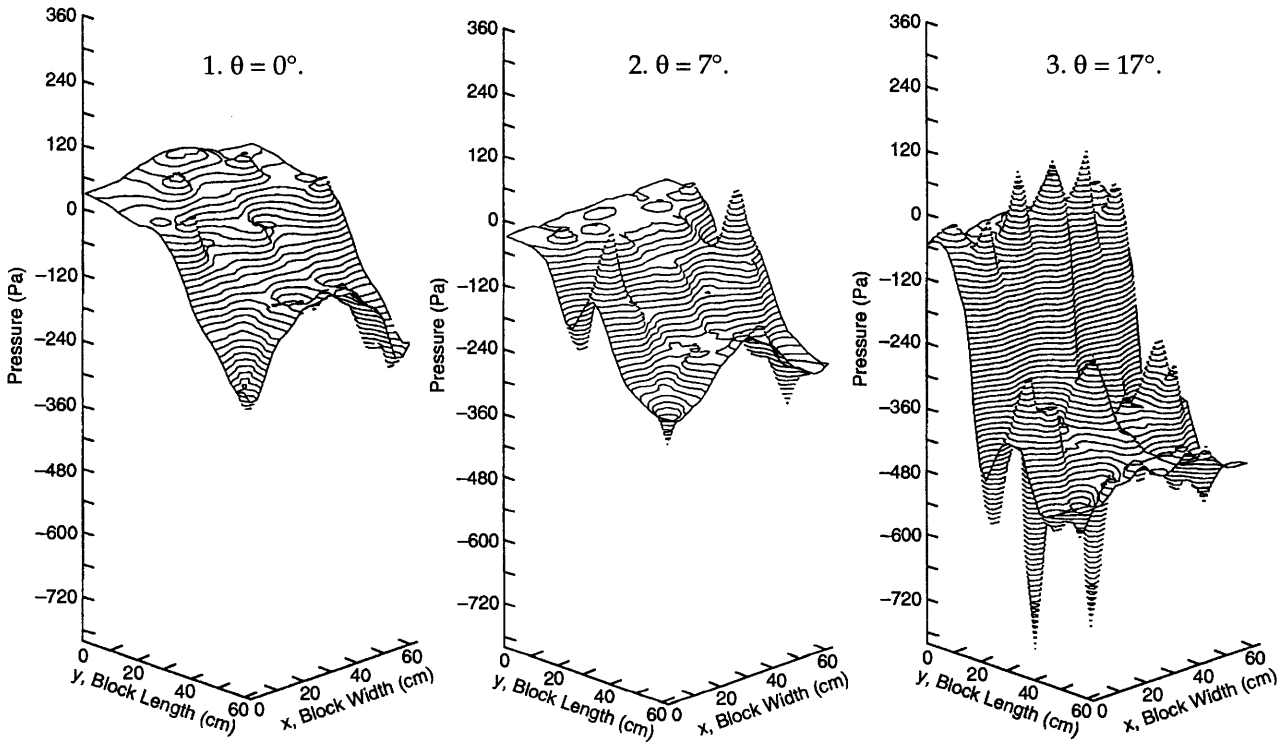

c. Test 3: t/H = *0.20,* V = *0.50 m/s.*

Figure 8 (cont'd). Representative pressure distributions from three tests. The block's trailing edge is at Y = *0.*

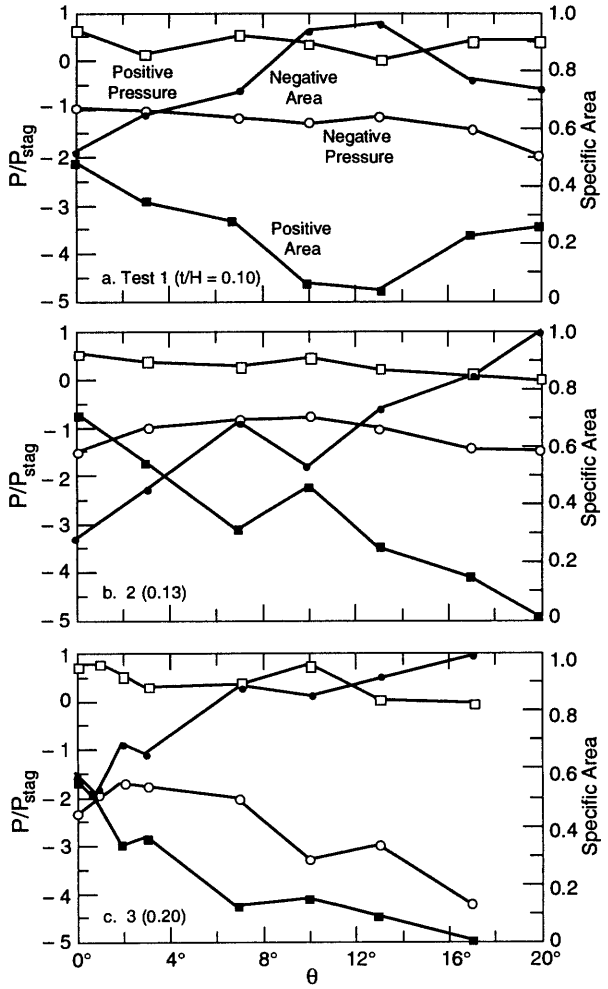

Figure 9. Areas of positive and negative pressure on the block's lower face, made nondimensional by the total block area. Also shown are the average pressures, made nondimensional with the stagnation pressure of the flow.

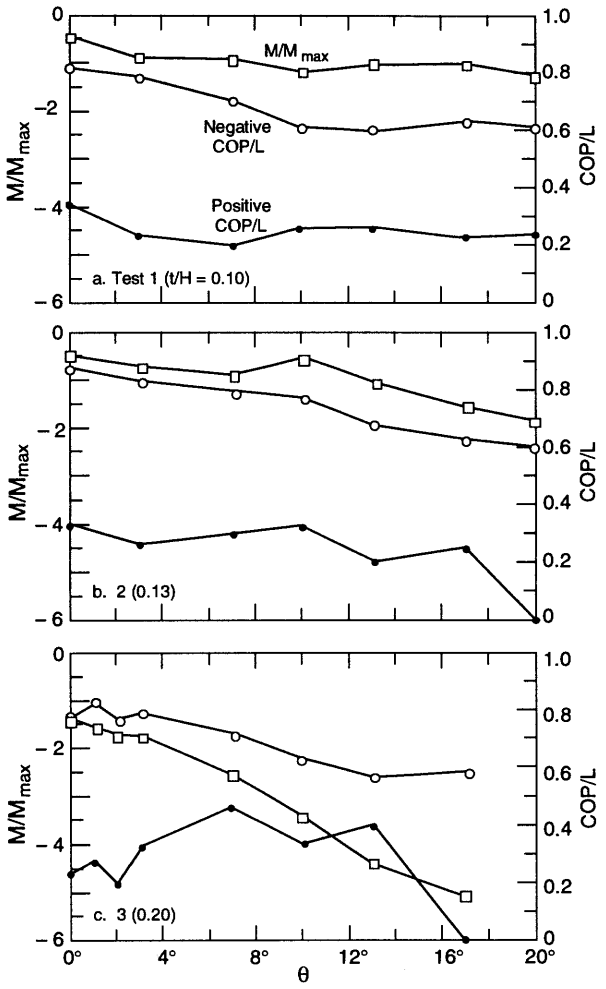

Figure 10. Center of negative and positive pressure divided by block length along with the total underturning moment, made nondimensional by the maximum hydrostatic righting moment (COP/L = 0 is the axis of rotation).

that the positive *COP*s in tests 1 and 2 are almost identical, while that for test 3 moves away from the rotation axis. This has the effect of hindering the block's rotation if we assume a pinned lower corner.

Since we assume that the block rotates about its downstream lower corner, these positive and negative pressures cause moments about that point. We therefore use our moment coefficient α as an indication of the total moment generated by the pressures about that axis. Figure 11 shows α plotted against angle of attack. There is an obvious trend of increasing α with increasing angle of attack. This trend is exaggerated in shallow water ($t/H = 0.20$) but is still present in the deeper water. There also appears to be a weak trend of decreasing α with increasing velocity at any fixed t/H ratio. Overall, depth seems to have a larger influence upon α than does velocity, showing a trend of decreasing α with increasing depth.

To see if the block is stable, we compare the measured moments attributable to dynamic fluid pressure with the block hydrostatic righting moments in Figure 12. Both the measured underturning moment and the righting moment are made nondimensional by the maximum righting moment given by eq 13. Also, the data are presented with the 95% confidence interval, which quantifies the uncertainty in our static pressure and individual tap readings. This uncertainty will be discussed below.

It can be seen from Figure 13 that the moments created on the block in the deeper water ($t/H = 0.10$ and $t/H = 0.13$) would not be sufficient to overcome the righting moment. At zero angle of attack, the moment would start the block rotating, but at the next measured angle, the moment is below the righting moment curve, which means it would be stable. Neglecting rotational inertia, we see that the block is stable if the underturning moment is not al-

ways greater than the righting moment. In the shallow water ($t/H = 0.20$), however, the moments generated at every velocity of our experimental program would be sufficient to underturn the block.

DISCUSSION

Data uncertainty

Inspection of the uncertainty shown in Figure 12 reveals an interesting trend. At $t/H = 0.20$ (shallow water), the uncertainty is generally uniform and

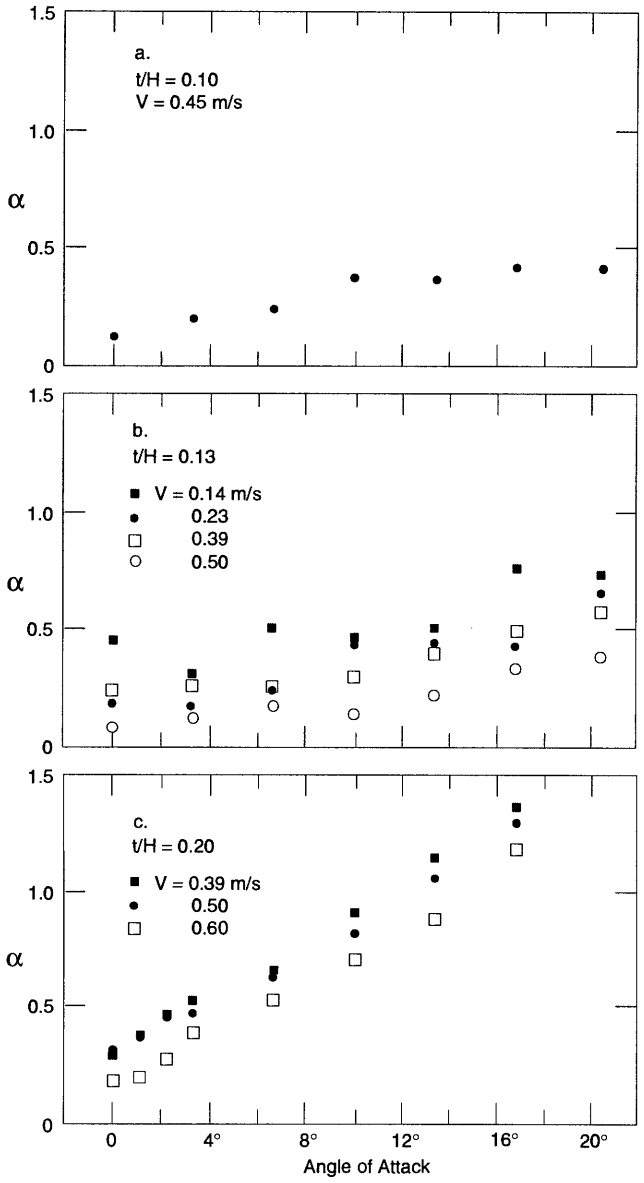

Figure 11. Nondimensional moment coefficient vs. angle of attack.

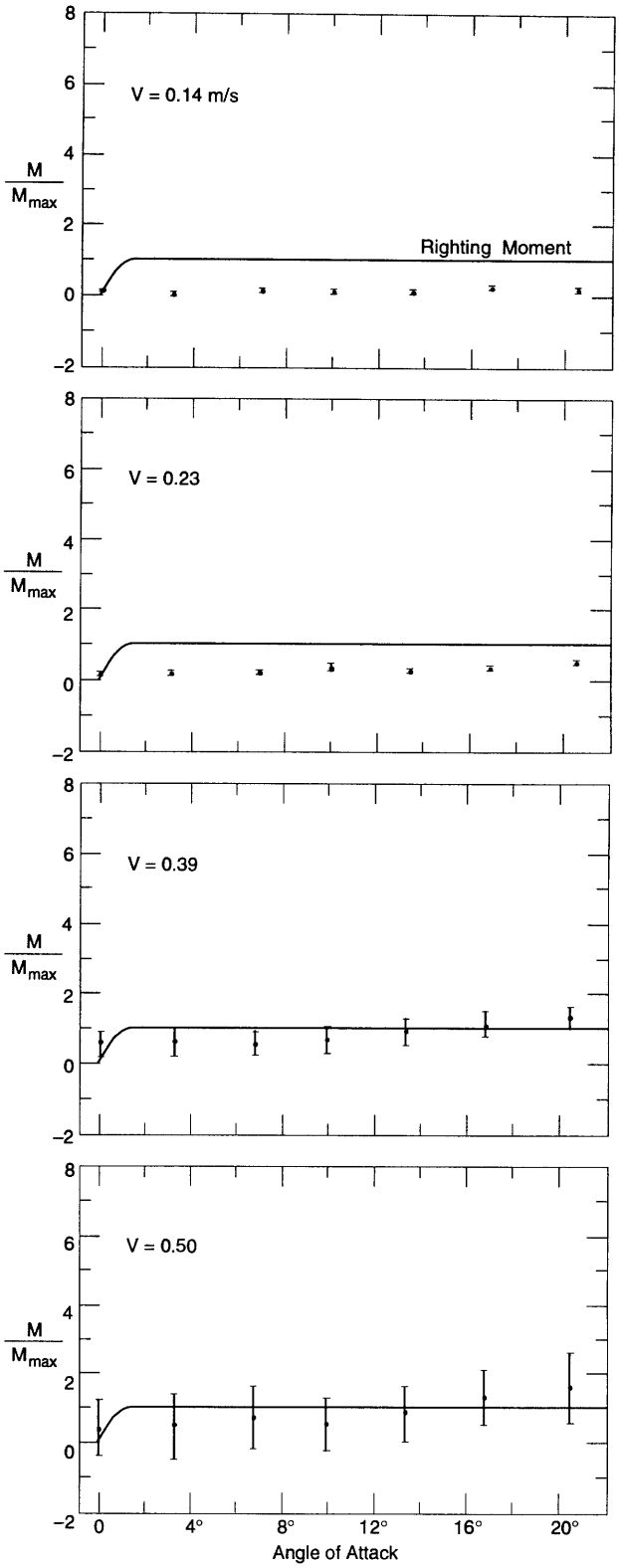

a. t/H= *0.13.*

Figure 12. Nondimensional underturning moment vs. angle of attack.

small. In the moderate depth water of $t/H = 0.13$, a slightly increasing uncertainty interval is evident with increasing velocity. In our deepest water experiments at $t/H = 0.10$, Figure 12c shows that the scatter is larger and takes a discontinuous jump at an attack angle of 13.4°.

We believe the generally larger uncertainty is caused by vibration in our experimental setup at high volumetric flow rates. Our block was attached to a frame that was in turn attached to the flume side walls. At the deeper water condition of $t/H = 0.10$ and $V = 0.45$ m/s, the high-frequency pump vibration was transmitted by the flume piping to the flume walls and thus to our block. The vibration was periodic and manifested itself as an increase in the calculated standard deviation of the differential pressures. We believe that the accuracy of the average values was not affected because we were able to analyze the readings in real-time during each experiment to ensure that the sampling rate was adequate for the vibration frequency. Our replicate values used to obtain the average shown in the figures are close to each other. In the worst-case deep water tests, the average difference between the replicates and the averaged M/M_{max} values was 39%, ranging down to less than 10% for the shallow water tests, giving us confidence in the procedure.

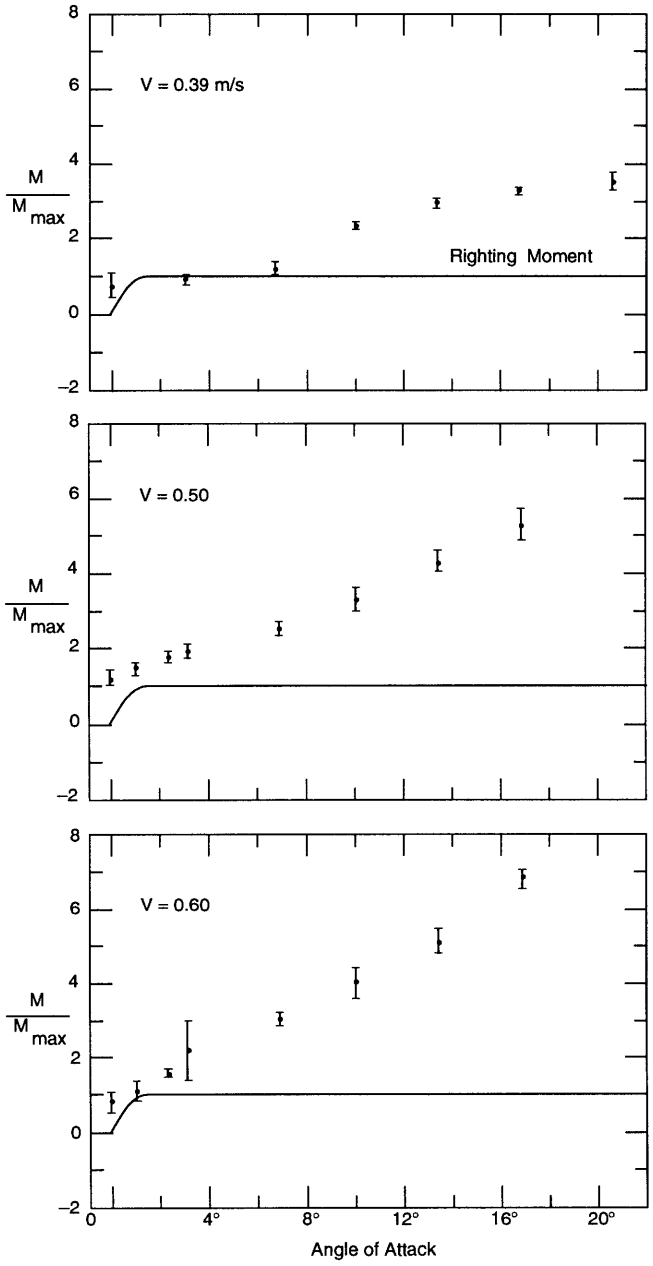

b. t/H = *0.20.*

Static analysis of block underturning

Using the above results, we look at block underturning through a static moment analysis, assuming a clockwise rotation as positive, and knowing that for a rotating block

$$\Sigma M > 0 \tag{15}$$

where M is a moment acting on the block. We express these moments as a function of block angle of attack θ by

$$M_f(\theta) - M_r(\theta) > 0 \tag{16}$$

with M_f being the underturning moment created by the fluid flow and M_r the hydrostatic righting moment. By neglecting the inertial component, we

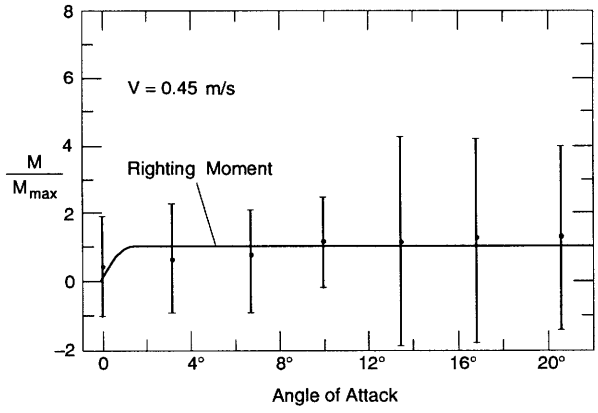

c. t/H = *0.10.*

Figure 12 (cont'd).

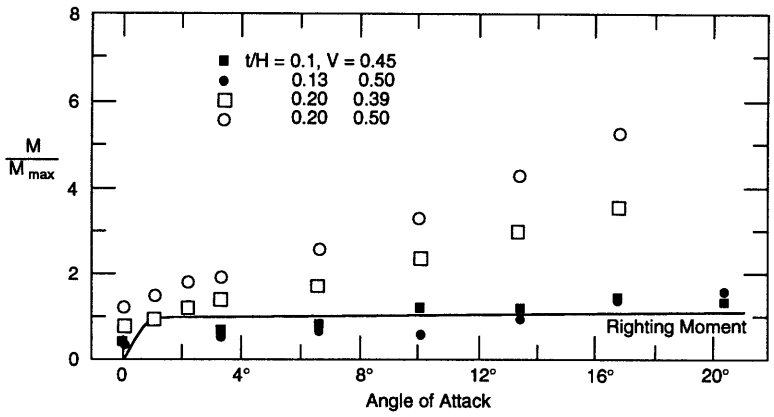

Figure 13. Nondimensional underturning moments vs. angle of attack for different t/H ratios at similar velocities.

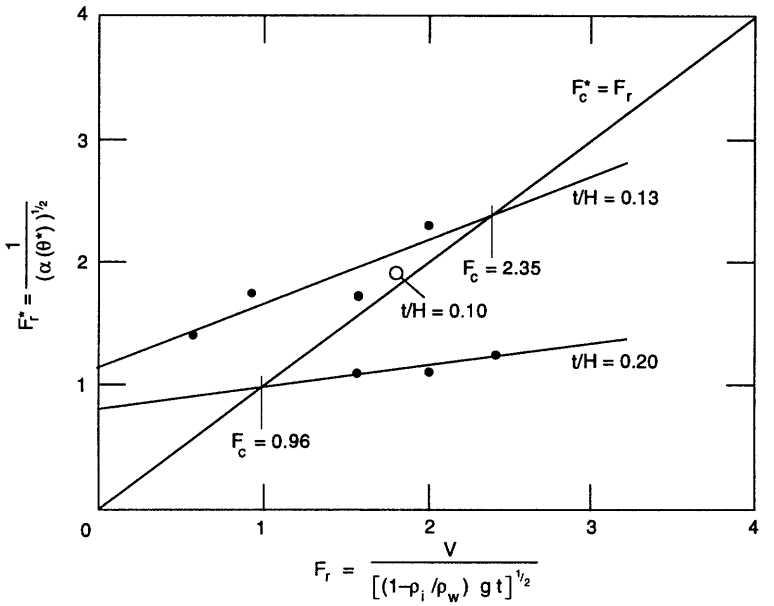

Figure 14. Froude criterion for block stability.

have a block instability criterion for all angles that will under-predict when a block becomes unstable, that is

$$\left(\frac{M_f(\theta)}{M_r(\theta)}\right) > 1 . \tag{17}$$

By inspection of the data, we can see that the underturning moment is linear through the angle where the hydrostatic righting moment is a maximum. This allows us to restrict eq 17 to θ^*, the angle of maximum righting moment, or

$$\left(\frac{M_f(\theta^*)}{M_r(\theta^*)}\right) > 1 . \tag{18}$$

With substitution of eq 2, 5, 6, and 13 into eq 18, we arrive at

$$M_f(\theta^*) = \left[\frac{1}{2} C(\theta^*) \rho_w V^2\right](A)\left[COP_Y(\theta^*)\right] \tag{19}$$

and

$$M_r(\theta^*) \approx \left\{\left[1-\left(\frac{\rho_i}{\rho_w}\right)\right]\rho_w g t\right\}(A)\left(\frac{L}{2}\right) \tag{20}$$

where ρ_i is ice density and g is the acceleration of gravity. The data indicate that for a particular t/H, both C and COP_Y are functions of the angle of attack θ. Taking this into account and substituting eq 19 and 20 into 18, we arrive at the expression

$$\left(\frac{V}{\left(\left(1-\left(\frac{\rho_i}{\rho_w}\right) g t\right)^{\frac{1}{2}}\right)}\right)\left(\frac{C(\theta^*)(COP_Y(\theta^*))}{L}\right)^{\frac{1}{2}} > 1 \tag{21}$$

which in the form of a densimetric Froude number (F_r) is as follows

$$F_r[\alpha(\theta^*)] > 1 . \quad (22)$$

And by defining

$$F_r^* = \frac{1}{(\alpha(\theta^*))^{\frac{1}{2}}} \quad (23)$$

we know that for block stability F_r must be less than F_r^* at any given t/H value. In Figure 14, F_r^* is plotted against F_r at t/H = 0.13 and t/H = 0.20 along with a line fit to the points by linear regression. Our one data point at t/H = 0.10 is included but was not used to find the regressed line. The 45° line depicts the critical Froude number for stability. The effect of the depth change on F_r^* between t/H = 0.20 and t/H = 0.13 is very evident, while increasing the depth from t/H = 0.13 to t/H = 0.10 would appear to have no effect. At t/H = 0.20, F_r^* is less sensitive to velocity than at t/H = 0.13. We would expect that more data at t/H = 0.10 would show little, if any, change from t/H = 0.13.

Dynamic analysis of block underturning

Figure 15 shows the moment coefficient as a function of block angle of attack θ for three thickness-to-depth ratios and several velocities. By neglecting the velocity dependence, the moment coefficient becomes a function of angle of attack and thickness-to-depth ratio (Fig. 16). A cubic polynomial fit of the moment coefficient was made to represent the data as a continuous function of angle of attack (in degrees). The curve fit takes the form

$$\frac{M_u}{\frac{1}{2}\rho_w g t A} = A_0 + A_1\theta + A_2\theta^2 + A_3\theta^3 \quad (24)$$

with the coefficients shown in Table 2.

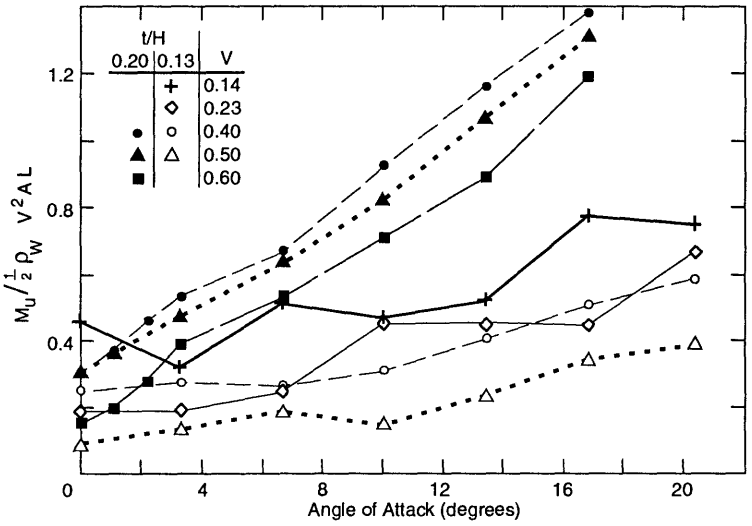

Figure 15. Moment coefficient for two thickness-to-depth ratios and several velocities.

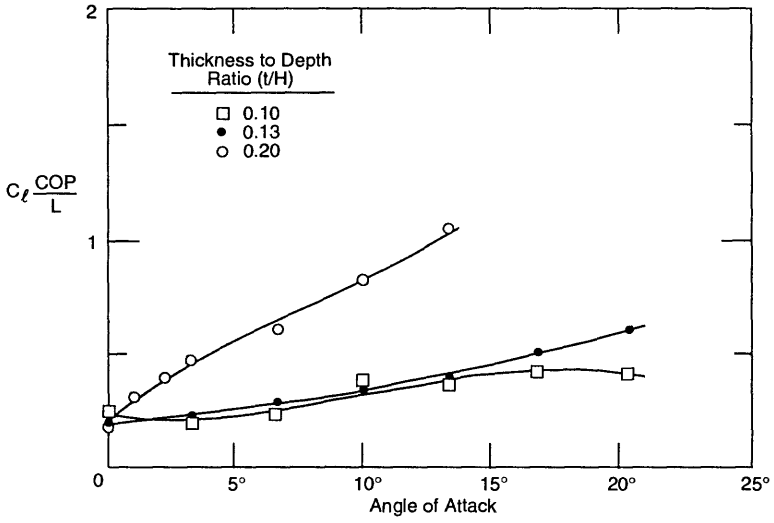

Figure 16. Cubic polynomial curve fit of moment coefficients to block angle of attack.

Table 2. Cubic polynomial curve fit of moment coefficient with angle of attack in degrees.

t/H	A_0	A_1	A_2	A_3	R^2
0.10	2.33×10^{-1}	-1.63×10^{-2}	3.75×10^{-3}	-1.24×10^{-4}	0.922
0.13	1.96×10^{-1}	9.56×10^{-3}	4.73×10^{-4}	8.48×10^{-7}	0.994
0.20	2.04×10^{-1}	8.67×10^{-2}	-4.49×10^{-3}	1.90×10^{-4}	0.998

Moment analysis

The equation for the motion of the block is

$$\Sigma M = I\ddot{\theta} \tag{25}$$

where the moment of inertia I is given by

$$I = \frac{1}{3}\rho_i LA\left(L^2 + t^2\right) \tag{26}$$

subject to the initial conditions

$$\theta_0 = 0$$

$$\dot{\theta} = 0$$

$$\ddot{\theta} = \frac{M_u(\theta_0) - M_r(\theta_0)}{I}. \tag{27}$$

In the expression for the moment of inertia, we have made the assumption that fluid inertia may be neglected. Our pressure measurements quantified the acceleration of the fluid around the block; therefore, we are neglecting only the fluid acceleration associated with block angular velocity and acceleration. This is reasonable because the upstream flow velocity was estimated to be approximately five times greater than the maximum velocity of the block leading edge as it rotates, which means that the fluid acceleration through time is relatively small compared to the acceleration in space. An estimate of the fluid added mass would require a knowledge of the volume of recirculating flow, which changes with both time and angle of attack. Such an estimate would be challenging while giving only marginal improvement in the solution of eq 25.

It is useful to define the external work done on the block by the fluid. If a mechanical energy balance is done on an ice floe that is initially at rest, we find that the cumulative work done on the block is equal to the rotational energy of the block. Formally, this is expressed as

$$\frac{1}{2}I\dot{\theta}^2 = \int_0^{\theta}\left(M_u - M_r\right)\partial\theta. \tag{28}$$

Evaluation of eq 28 leads to the five characteristic energy curves shown in Figure 17. Each kinetic energy curve is shown with its corresponding righting and underturning moments. Figure 17a shows that the underturning moment is greater than the righting moment for all angles considered. This condition leads to unequivocal block instability, as is evidenced by the continuously increasing kinetic energy curve.

Upon lowering the velocity, the underturning moment becomes tangent to the righting moment at exactly one point, as is shown in Figure 17b. At the point of tangency, the kinetic energy curve achieves a point of inflection where the angular acceleration equals 0. In the absence of rotational inertia, the block would remain at this angle of attack, since the underturning moment equals the righting moment. A somewhat lower velocity leads to a righting moment in excess of the underturning moment, which means that the block would be stable. A higher velocity would lead to a larger underturning moment, which means that the block would be unstable. Therefore, this represents the point of static metastability.

Figure 17c shows the effect of a further reduction in approach velocity. In this case, the block achieves a local maximum in kinetic energy at the first intersection of underturning moment and righting moment. Then, the righting moment is greater than the underturning moment, leading to a slowing of the block, as is evidenced by a reduction in block kinetic energy. Finally, at the second intersection of the righting and underturning moments, the kinetic energy achieves a local minimum. Beyond this point, the block is unstable. Clearly, it is the block rotational inertia that carries the block through these angles where the righting moment exceeds the underturning moment.

If we reduce the velocity still further (Fig. 17d), the block again achieves a local maximum in kinetic energy, but this time the local minimum occurs at a kinetic energy of 0. This means that the block has been brought to rest at a positive angle of attack where the underturning moment equals the righting moment. This point represents a metastable position, since a perturbation in velocity will either render the block stable or unstable. Therefore, this velocity and angle of attack may be considered critical to dynamic block stability.

Finally, we reduce the velocity to achieve the stable condition shown in Figure 17e. In this case, the block picks up angular momentum and achieves a local maximum in kinetic energy as before. However, the kinetic energy of the system never achieves

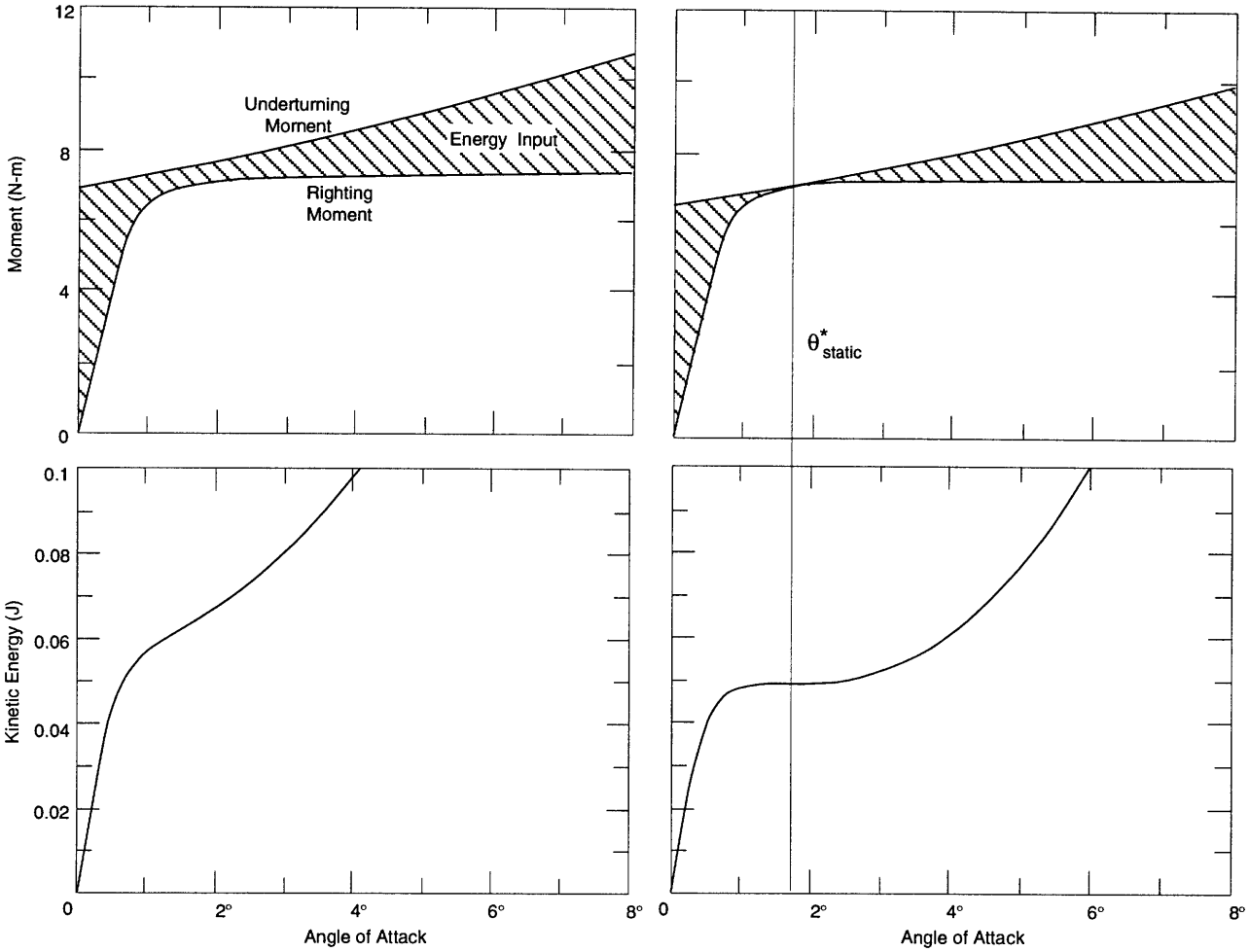

a. Unstable block at t/H = *0.13 and* V = *0.55 m/s.*

b. Static metastability at t/H = *0.13 and* V = *0.53 m/s.*

Figure 17. Characteristic energy curves.

a local minimum. Instead, it becomes equal to zero at an angle where the righting moment exceeds the underturning moment. This condition can cause the block to oscillate stably in this range of angular displacement.

To evaluate the effect of rotational inertia on block stability, we define the densimetric Froude number at metastability F_r^* as

$$F_r^* = \frac{V^*}{\sqrt{\left(1-\frac{\rho_i}{\rho_w}\right)gt}} \tag{29}$$

with V^* taking on a value associated with Figure 17b for static stability criteria and Figure 17e for dynamic stability criteria. An iterative procedure was implemented to determine the velocity that gave the proper conditions for both static and dynamic stability.

Comparison with previously published results

Other investigators have given block stability criteria that may be compared with the current analysis. Pariset and Hausser (1961) gave the following stability criterion in the form of a Froude number with depth as the characteristic length scale. Their equation is

$$\frac{V}{\sqrt{2gH}} = \kappa\sqrt{\left(1-\frac{\rho_i}{\rho_w}\right)\left(\frac{t}{H}\right)\left(1-\left(\frac{t}{H}\right)\right)} \tag{30}$$

where H = upstream depth of flow
V = approach velocity
κ = empirical parameter.

The parameter κ is not used in a later paper by Pariset et al. (1966).

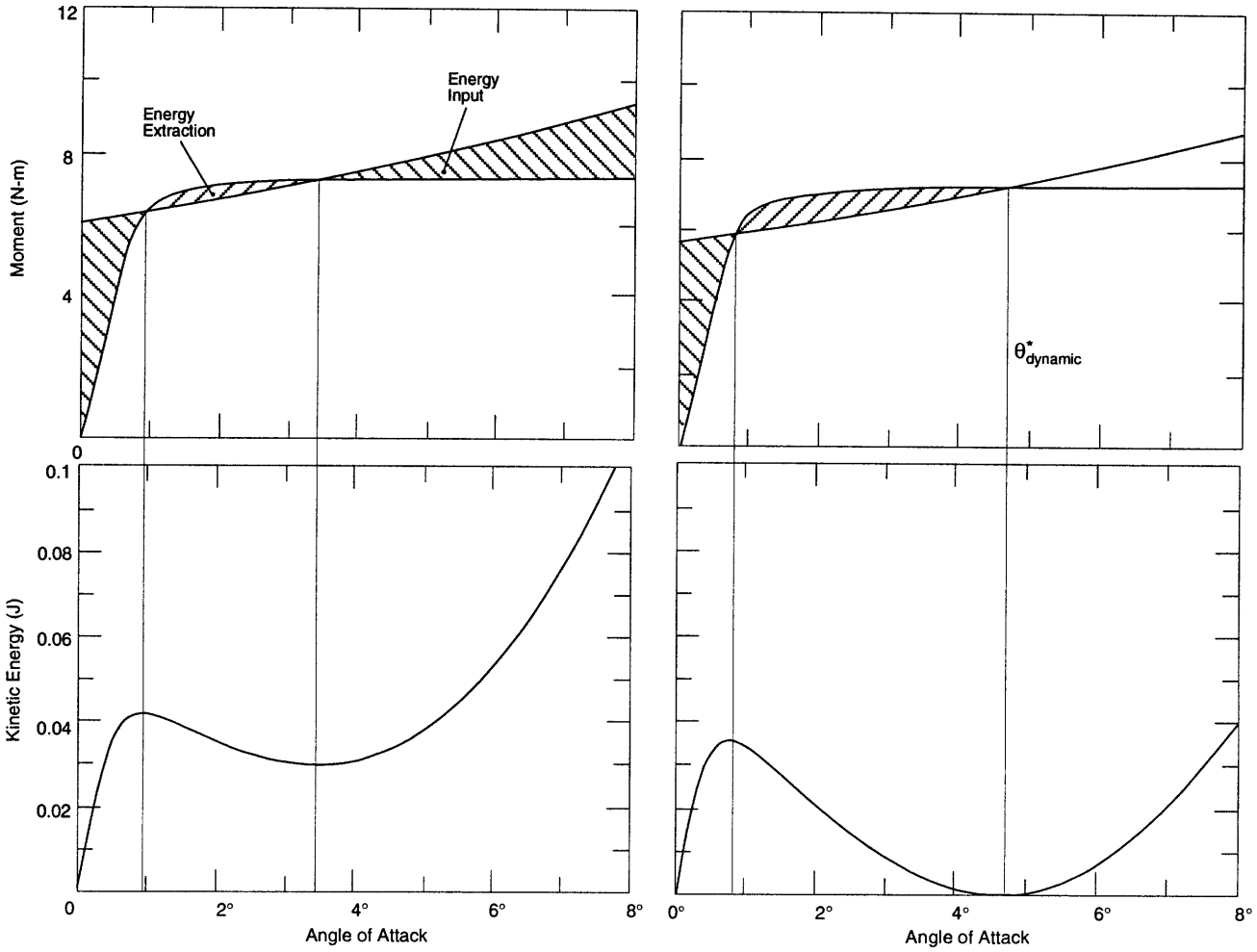

c. Unstable block at t/H = *0.13 and* V = *0.51 m/s.*

d. Metastable block at t/H = *0.13 and* V = *0.50 m/s.*

Figure 17 (cont'd). Characteristic energy curves.

Ashton's stability criterion is in the form of a densimetric Froude number

$$\frac{V}{\sqrt{gt\left(1-\frac{\rho_i}{\rho_w}\right)}} = \frac{2\left(1-\frac{t}{H}\right)}{\sqrt{5-3\left(1-\frac{t}{H}\right)^2}}. \qquad (31)$$

Daly (1984) introduced a shallow-water stability criterion of the form

$$\frac{V}{\sqrt{gt}} = \frac{\left(\sqrt{4/3}\right)\left(1-\frac{t'}{H}\right)\beta}{\sqrt{1-\left(1-\frac{t'}{H}\right)^2-\left(\frac{t}{H}\right)\left(\frac{t}{L}\right)^2(\rho')^3}} \qquad (32)$$

where t' is block freeboard and β is an empirical fitting constant equal to 0.27. For deep water conditions, Daly used

$$\frac{V}{\sqrt{gt}} = \frac{S_t{}^{\pm 1}}{\sqrt{\frac{\rho_i}{\rho_w}\left(1+\left(\frac{t}{L}\right)^2\right)}} \qquad (33)$$

where S_t is the Strouhal number at block instability, and may be determined from the data.

In Coutermarsh (1986), a value of 2.08 was assumed for a wide variety of block geometries, while in the current work a value of 1.78 is used. Figure 18 shows these stability criteria and the critical Froude numbers determined from the current analysis. As can be seen, both Pariset and Hausser's and Ashton's stability criteria under-predict the critical Froude number for the block geometry under consideration.

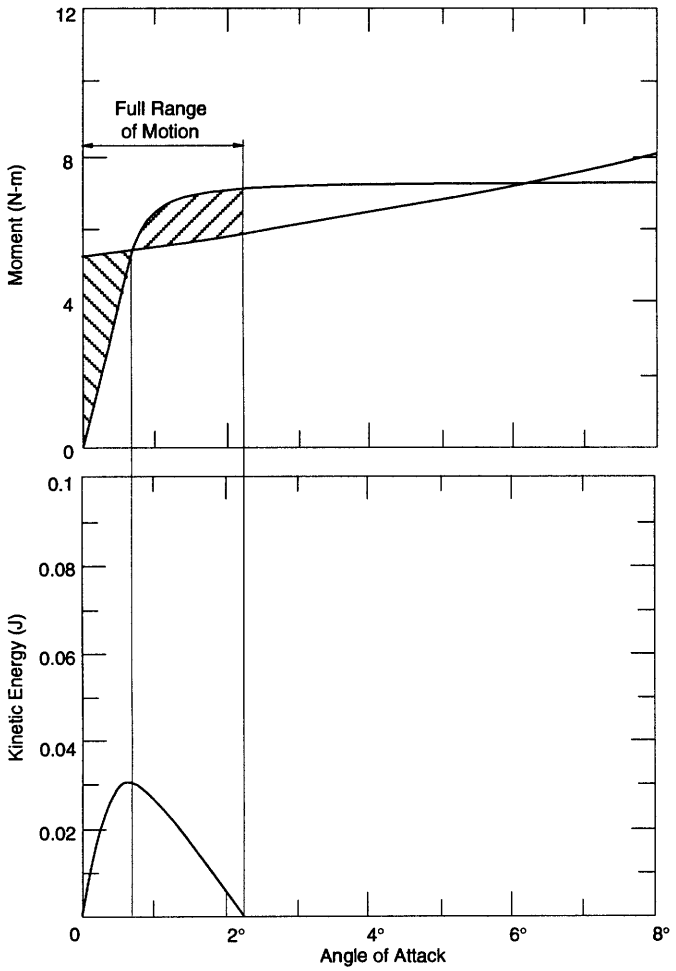

e. Stable block at t/H = *0.13 and* V = *0.48 m/s.*

Figure 17 (cont'd).

Daly's criterion does reasonably well in predicting both the deeper-water and the shallow-water cases. However, if Daly's deep-water criterion is used with a Strouhal number of 2.08, it also underpredicts the critical Froude numbers. Because in the current work we neglect the effects of hydrodynamic fluid pressure on the top of the block and on the front face, the block is expected to underturn at slightly lower Froude numbers than those calculated. Indeed, fluid pressure on the top of the block would reduce the difference between the calculated critical Froude number and Daly's predictions based on a Strouhal number of 2.08. In any case, the Strouhal number is a function of block geometry, and a variation between 2.08 and 1.78 is possible, given the differences in block geometry. The most salient feature of the deep water data is an apparent leveling off of the critical Froude number with decreasing thickness-to-depth ratio. This has an intuitive appeal since we expect that the moment coefficient should become completely insensitive to arbitrary increases in fluid depth for very deep water conditions. The current work, coupled with Daly's deep-water criterion, lends support to this argument.

It is difficult to know exactly how well Daly's criterion represents the shallow-water data since we have only one such data point. In spite of this drawback, Daly's criterion does appear to represent the expected trend reasonably well. More data are required before a definite conclusion may be drawn about his shallow-water criterion.

An important feature of Figure 18 is the offset between the static and dynamic Froude numbers re-

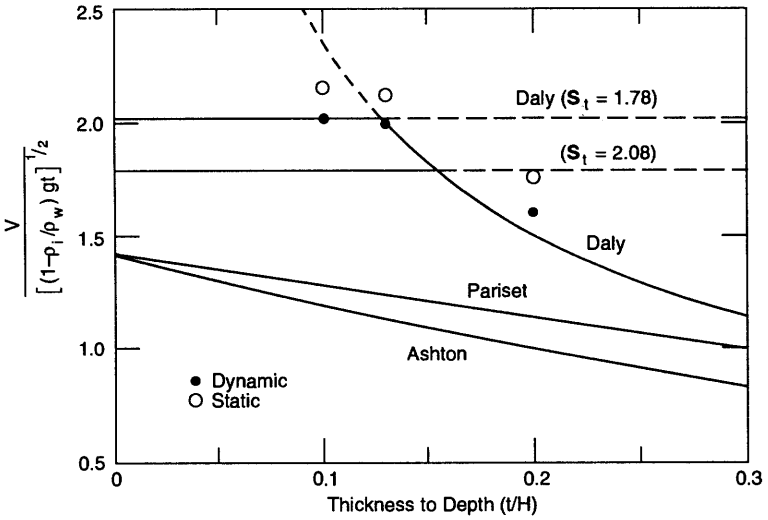

Figure 18. Comparison of calculated stability points with existing stability criteria.

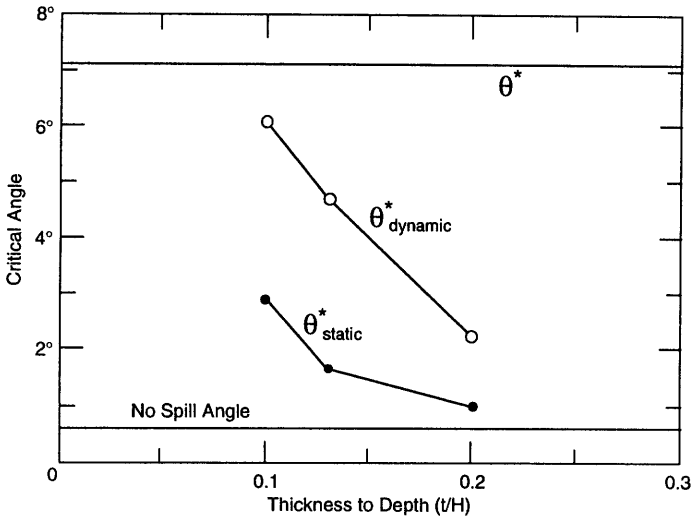

Figure 19. Angles at which the model ice floe achieves metastability.

quired to destabilize the block. Evidently, for these thickness-to-depth ratios and block geometry, fluid inertia is responsible for a 5 to 10% decrease in the Froude number to destabilize the block. Furthermore, we expect a further 5 to 10% decrease in critical Froude number by including the hydrodynamic fluid forces on the top and front face of the block, which have been ignored in the current work.

Figure 19 shows the angle at which metastability occurs. This angle is compared to other often-cited angles such as the no-spill angle and the angle of maximum righting moment. The angle of static metastability is lower than the angle of dynamic metastability because of how each is defined. Static metastability occurs at the point of tangency of the righting and underturning moments. Dynamic metastability occurs at the second intersection of righting and underturning moments that gives zero block kinetic energy. These conditions are shown graphically in Figures 17b and d.

It is interesting to note that at deep water conditions the angle of maximum righting moment may be very close to the angle of dynamic metastability, while at very shallow water conditions the classic no-spill angle may be very close to the metastability angle. More data are required before these relationships may be established.

The angle at which metastability occurs may have little practical importance except to guide further research that focuses on measuring the underturning–righting moments at various angles of attack. For example, it appears that for this block-length-to-thickness aspect ratio and density, angles greater than 10° need not be considered in an experimental program. Although it is unknown how well these angles would hold for other block geometries, it appears that the upper limit is not far from the angle at which the maximum righting moment occurs.

CONCLUSIONS

The hydrodynamic fluid pressures beneath an idealized, parallelepiped model ice block were measured. The ice block was fixed in space, thereby eliminating angular acceleration during measurement of the fluid pressures. The pressure distribution was shown to be symmetrical about the centerline of the block and included regions of positive (stabilizing) pressure and negative (underturning) pressure. The net underturning moment for the entire pressure distribution was compared with the hydrostatic righting moment, and the condition of static stability was described. A flow area reduction, which includes the thickness-to-depth ratio, the length-to-depth ratio and the angle of attack, is presented. A moment coefficient was defined that relates the magnitude and point of application of the dynamic fluid pressures. It is evaluated in relation to flow depth and flow velocity for a fixed block geometry. The moment coefficient appears to have a linear relationship with the reduction ratio over the range of parameters investigated. This linear relationship suggests that block length is as important as thickness for characterizing block stability in deep water conditions, especially for high L/t aspect ratio blocks.

The underturning phenomenon is related to the described hydrostatic righting moment of the block, which depends on block geometry and density and fluid density. By combining the two phenomena, we arrive at a block underturning description in terms of moments. We have shown that this block underturning can be described by a relatively simple equation that relates a Froude number to block instability. Furthermore, if the block were not constrained at its lower downstream corner, the couple developed by the fluid forces would tend to rotate it with less effort by uplifting the rear of the block. This, along with our not including any rotational inertia effects in the above, means we have a moment analysis that will somewhat under-predict when a block will underturn.

Our dynamic analysis of stability shows that ice floe angular momentum may lead to rotational instability even when the righting moment is greater than the underturning moment at a given angle of

attack. In this analysis, the net work on the block was equated to the rotational kinetic energy of the block. This yielded estimates of stability for the model ice floe for three thickness-to-depth ratios, which were shown to compare favorably to an existing stability criteria. The angular momentum causes block instability at Froude numbers 5 to 10% below those associated with static stability. The calculated Froude numbers are assumed to over-predict the actual critical Froude numbers since the hydrodynamic pressure distribution on the top and front of the model ice floe was not measured.

The measured areas of positive pressure at the back of the block suggest that it is possible for a block to be pushed out of the water vertically at its downstream edge. Researchers* we have spoken with have confirmed seeing this phenomenon.

We were constrained in our ability to present a complete set of moment coefficients by our limited experiments. Future work in this area would do well to investigate different block thickness-to-depth ratios and block lengths. The three-dimensional pressure distributions also suggest that the effect of block width should be investigated. Consideration of blocks with rounded leading edges might also prove interesting to see the variation in flow attachment. Better flow visualization may also shed light on the phenomenon of positive pressures beneath the ice block.

Deep water data ($t/H > 0.10$) at velocities over 0.45 m/s would be interesting and should be obtained. We were restricted in both available depth and achievable velocities in our facilities. We, therefore, could not fully characterize the deeper flows.

As mentioned before, our experiments did not include any effect attributable to the dynamic fluid impact against the front and top of the block. Experiments that measure force on the block at a known distance from the assumed rotation point would contain this information, although they would not reveal the nature of the forces.

* Personal communication with Dr. G. Ashton and Dr. J. Lever, both of CRREL, 1991.

Because one of the ultimate goals of this work is to estimate the capture efficiency of an ice cover, future efforts should also be focused on characterizing the typical ice floe geometries found in the field and then quantifying the righting and underturning moments associated with these geometries.

Additionally, the initial impact of an ice floe with an ice cover may be destabilizing and should be investigated as a separate issue. With all of the desired data, a family of curves could be developed to more fully document the capture efficiencies for a distribution of geometries and range of flow conditions. Such calculations would be useful for designers and operators of ice control structures, as well as for numerically modeling the behavior of floating ice floes.

LITERATURE CITED

Ashton, G.D. (1974) Froude criterion for ice block stability. *Journal of Glaciology*, **13**(68): 307–313.

Coutermarsh, B.C. (1986) Model studies of ice interaction with the U. S. Army Ribbon Bridge. USA Cold Regions Research and Engineering Laboratory, CRREL Report 86-1.

Daly, S.F. (1984) Ice block stability. In *Proceedings, ASCE Hydraulics Division Conference on Water for Resource Development, 14–17 August.* New York: American Society of Civil Engineers.

Daly, S. and K. Axelson (1990) Stability of floating and submerged blocks. *Journal of Hydraulic Research*, **28**(6): 737–752.

Larsen, P. (1975) Notes on the stability of floating ice blocks. In *Proceedings of the Third International Symposium on Ice Problems*, p. 305–313.

Pariset, E. and R. Hausser (1961) Formation and evolution of ice covers on rivers. *Transactions of the Engineering Institute of Canada*, **5**(1): 41–49.

Pariset, E., R. Hausser and A. Gagnon (1966) Formation of ice covers and ice jams in rivers. *Journal of the Hydraulics Division, ASCE*, **92**: 1–24.

Streeter, V. and E. Wiley (1979) *Fluid Mechanics*, 7th edition. New York: McGraw-Hill, Inc., p. 42–44.

Uzuner, M. and J. Kennedy (1972) Stability of floating ice blocks. *Journal of the Hydraulics Division, ASCE*, **98**(HY12): 2117–2133.

REPORT DOCUMENTATION PAGE

Form Approved
OMB No. 0704-0188

1. AGENCY USE ONLY (Leave blank)	2. REPORT DATE	3. REPORT TYPE AND DATES COVERED
	December 1994	

4. TITLE AND SUBTITLE

Analyzing the Stability of Floating Ice Floes

5. FUNDING NUMBERS

6. AUTHORS

Barry Coutermarsh and Randy McGilvary

7. PERFORMING ORGANIZATION NAME(S) AND ADDRESS(ES)

U.S. Army Cold Regions Research and Engineering Laboratory
72 Lyme Road
Hanover, New Hampshire 03755-1290

8. PERFORMING ORGANIZATION REPORT NUMBER

CRREL Report 94-13

9. SPONSORING/MONITORING AGENCY NAME(S) AND ADDRESS(ES)

U.S. Army Cold Regions Research and Engineering Laboratory
72 Lyme Road
Hanover, New Hampshire 03755-1290

10. SPONSORING/MONITORING AGENCY REPORT NUMBER

11. SUPPLEMENTARY NOTES

12a. DISTRIBUTION/AVAILABILITY STATEMENT

Approved for public release; distribution is unlimited.

Available from NTIS, Springfield, Virginia 22161

12b. DISTRIBUTION CODE

13. ABSTRACT (*Maximum 200 words*)

This report describes an experimental study to measure the pressure caused by fluid acceleration beneath a floating parallelepiped block. Dynamic fluid pressure was measured at discrete points beneath the block for several flow velocities, flow depths, block angles of attack and block-thickness-to-depth ratios. The measured pressures were used to calculate block underturning moments, and a hydrostatic analysis was used to calculate a block righting moment. From this, a densimetric Froude underturning criterion is presented. The measured hydrodynamic pressure distribution on the bottom of a single model ice floe is used to estimate the dynamic stability at three thickness-to-depth ratios. The energy-based analysis details the conditions required for instability, metastability and stability. At three thickness-to-depth ratios, block rotational inertia has the effect of reducing the Froude stability number by 5 to 10% over a completely static stability criterion.

14. SUBJECT TERMS

Cold regions, Flume experiments, Ice, Ice blocks, Ice covers, River ice

15. NUMBER OF PAGES
28

16. PRICE CODE

17. SECURITY CLASSIFICATION OF REPORT	18. SECURITY CLASSIFICATION OF THIS PAGE	19. SECURITY CLASSIFICATION OF ABSTRACT	20. LIMITATION OF ABSTRACT
UNCLASSIFIED	UNCLASSIFIED	UNCLASSIFIED	UL